Supplementary information

Minimizing Two-Dimensional $Ti_3C_2T_x$ MXene Nanosheet Loading in Carbon-free Silicon Anodes

Kasturi T. Sarang[a], Xiaofei Zhao[a], Dustin Holta[b], Miladin Radovic[b], Micah J. Green[ab], Eun-Suok Oh*[c], Jodie L. Lutkenhaus*[ab]

[a]Artie McFerrin Department of Chemical Engineering, Texas A&M University, College Station, Texas 77843, United States

[b]Department of Material Science & Engineering, Texas A&M University, College Station, TX 77843, USA

[c]School of Chemical Engineering, University of Ulsan, Ulsan 44611, South Korea

Corresponding authors email ids

Dr. Jodie Lutkenhaus: jodie.lutkenhaus@tamu.edu

Dr. Eun-Suok Oh: esoh1@ulsan.ac.kr

Synthesis of Ti_3AlC_2 MAX phase

Ti_3AlC_2 MAX phase was synthesized from Ti (with a particle size of 44 μm and 99.5% purity), Al (with a particle size of 44 μm and 99.5% purity) and TiC (with a particle size of 2-3 μm and 99.5% purity) powders which were mixed in the molar ratio of Ti: Al: TiC=1.2:1.2:1.8. All chemicals were used as received from Alfa Aesar, MA, USA. The bulk high-purity Ti_3AlC_2 samples were synthesized by heating up the Ti+Al+TiC powder mixture in a tube furnace to 1510 ℃ at 10 ℃/min and being kept for 4 hours. After sintering, the highly porous bulk Ti_3AlC_2 samples were drill-milled to obtain Ti_3AlC_2 powder, which was then sieved to obtain the powder with particle size less than 45 μm.

Synthesis of $Ti_3C_2T_x$ MXene (MXs) clay

$Ti_3C_2T_x$ MXene clay was obtained by etching the Al layer from the sieved MAX phase by a wet etching method. 50 mL of 6 M hydrochloric acid (HCL) solution (ACS reagent, Sigma-Aldrich) and 3.0 g of lithium fluoride (LiF) (with the purity of 98+%, Alfa Aesar) were first mixed in a polypropylene bottle until all LiF was dissolved. The solution was heated to 35 °C before 5 g of as-prepared MAX powder was slowly added into the solution over 15 minutes to prevent overheating. The mixture was continuously agitated and reacted for 40 hours. Deionized water was used to wash the MXene clay repeatedly until pH of the water effluent reached a minimum value of 6.

Intercalation and delamination of MX clay

MXene clay was intercalated with dimethyl sulfoxide (DMSO) (>99.5%, Sigma-Aldrich) with agitation for 20 hours. After washing the DMSO away by distilled water, the MXene clay in water dispersion was bath sonicated for 60 mins to exfoliate into nanosheets. The delaminated dispersion was centrifuged at 3500 rpm for 1 hour to separate the unexfoliated MXenes and other heavier components. The supernatant containing the $Ti_3C_2T_x$ nanosheet dispersion was collected after centrifugation, while the sediment after centrifugation was discarded.

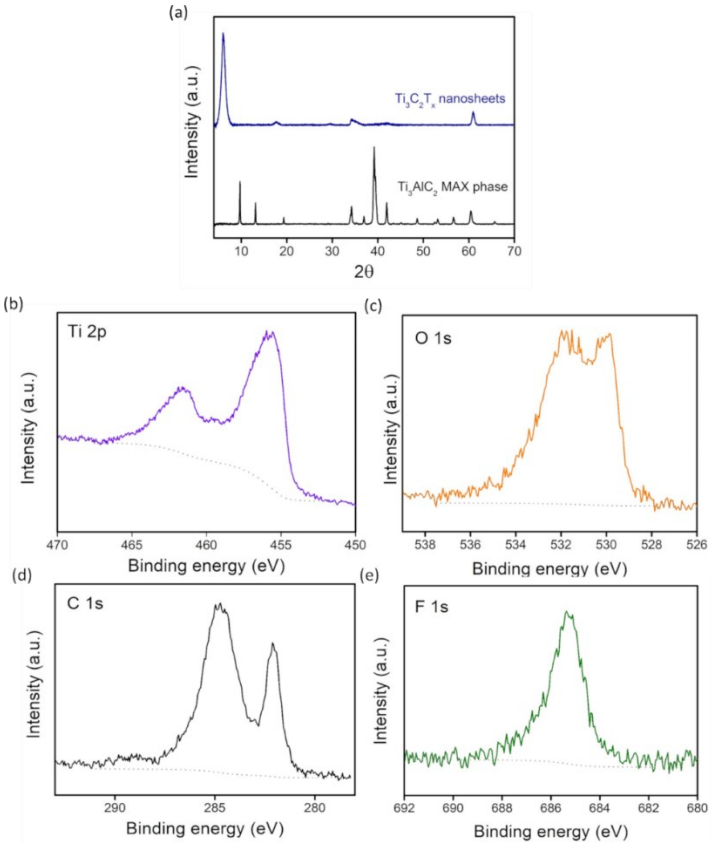

Figure S1. (a) X-ray diffraction spectra (XRD) of Ti_3AlC_2 MAX phase and $Ti_3C_2T_x$ MXene nanosheets (b)-(e) X-ray photoelectron spectroscopy (XPS) spectra of Ti 2p, O 1s, C 1s, and F 1s for the MXene nanosheets.

XRD patterns of MXene nanosheets were obtained using a Bruker D8 powder X-ray diffractometer with a CuKα (λ = 1.5418 Å) radiation source. The scan was performed with a step size of 0.02° and a scan rate of 1.5 s per step. The MXene film used for XRD was obtained by vacuum filtration. An Si zero-background sample holder was used in the test.

X-ray photoelectron spectroscopy (XPS) spectra were probed using an Omicron X-ray photoelectron spectrometer employing a Mg-sourced X-ray beam to irradiate sample surface. The photoelectrons emitted from sample surface were collected by a 180° hemispherical electron energy analyzer. During all scanning, charge neutralization by a dual beam charge neutralizer was performed to remove the low-energy electrons to eliminate the BE shifts in the recorded spectra. Samples for XPS measurements were prepared by freeze drying the $Ti_3C_2T_x$ dispersion. High resolution spectra of Ti 2p, C 1s, O 1s, F 1s were recorded at a pass energy (constant analyzer energy, CAE) of 30.0 eV with a step size of 0.05 eV.

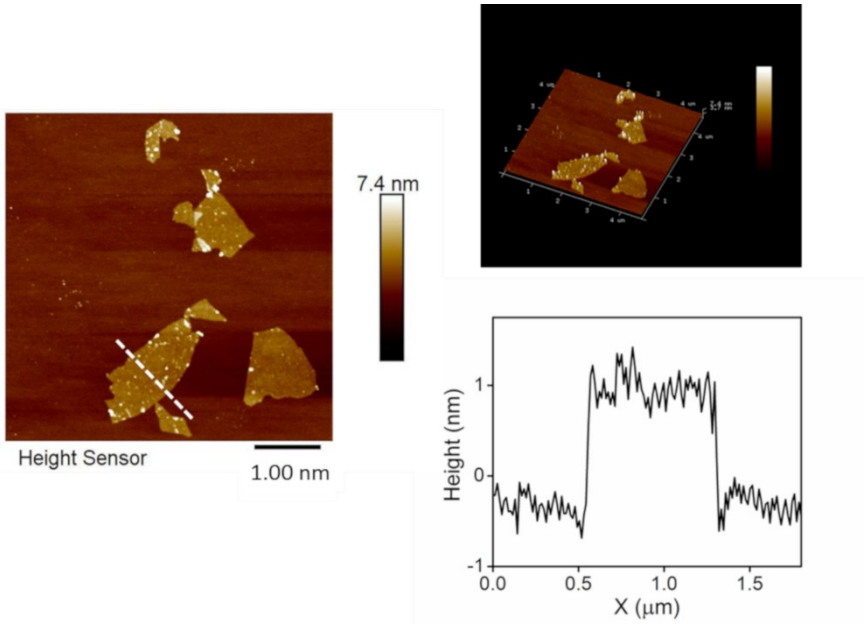

Figure S2. Atomic force microscopy (AFM) image of MXene nanosheets. MXene nanosheets had a lateral size of around 1 µm and a thickness around 1.2 nm. The sample tested using AFM was prepared by dropping casting the diluted MX dispersion on a freshly cleaved mica substrate. The sample dried overnight under vacuum at 40 °C. Height profiles of nanosheets were obtained in tapping mode (Bruker dimension icon AFM).

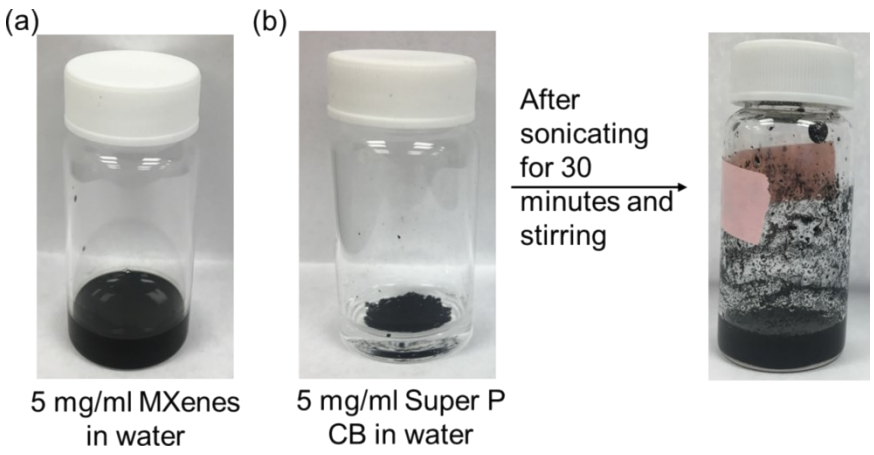

Figure S3. (a) Digital image of freeze-dried MXene nanosheets in 1 wt% sodium alginate solution in water. A minute of bath sonication is enough to form a stable dispersion of MXenes in water. (b) Digital image of super P carbon black (CB) in 1 wt% sodium alginate solution in water. Sonication and stirring for 30 minutes was required to somewhat disperse the Super P carbon black.

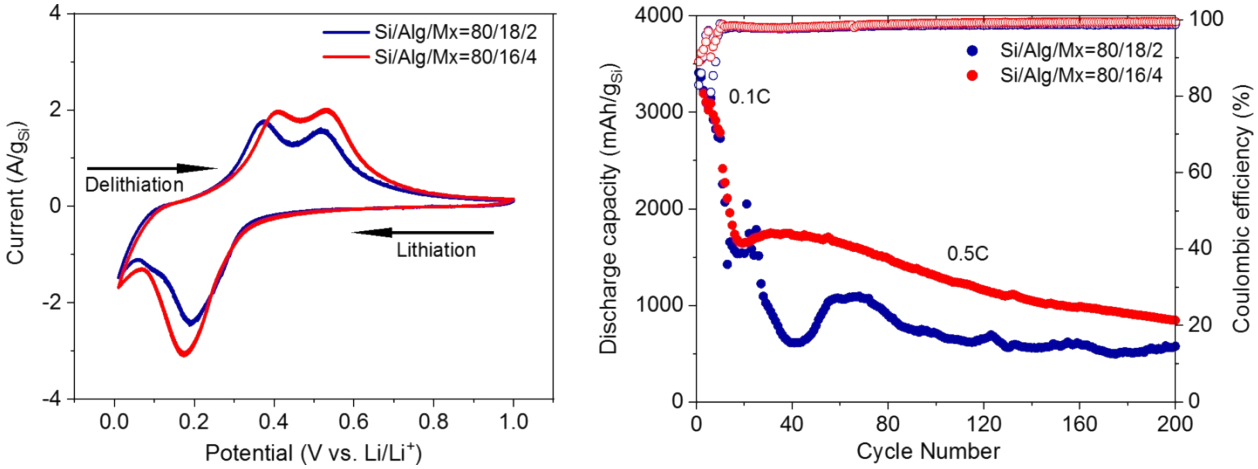

Figure S4. (a) Cyclic voltammogram at 0.1 mV/s (3rd cycle for each) and (b) cycling performance at 0.1 C in CC-CV mode for 1st five cycles followed by 0.5 C in CC mode for the remaining cycles. Electrodes with different MXene content were compared. Electrode with 4 wt% MXenes showed higher capacities than the one with 2 wt% MXenes.

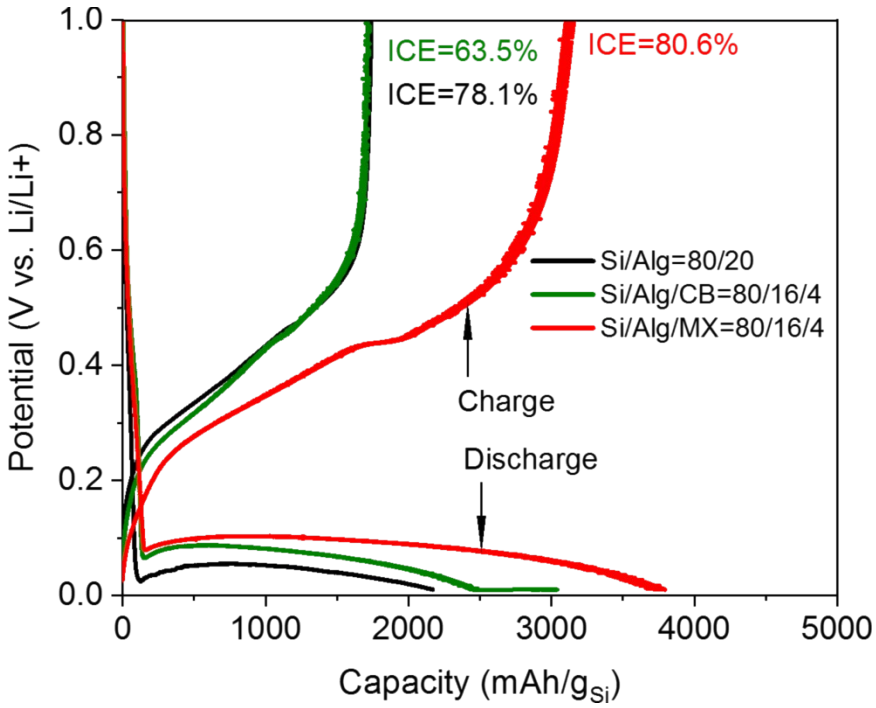

Figure S5. Voltage profile of Si/Alg=80/20, Si/Alg/CB=80/16/4, and Si/Alg/MX=80/16/4 for the 1st cycle at 0.1 C. Selected remaining cycles from 6th to 200th cycle at 0.5 C are shown in Figure 3b-d in the main text.

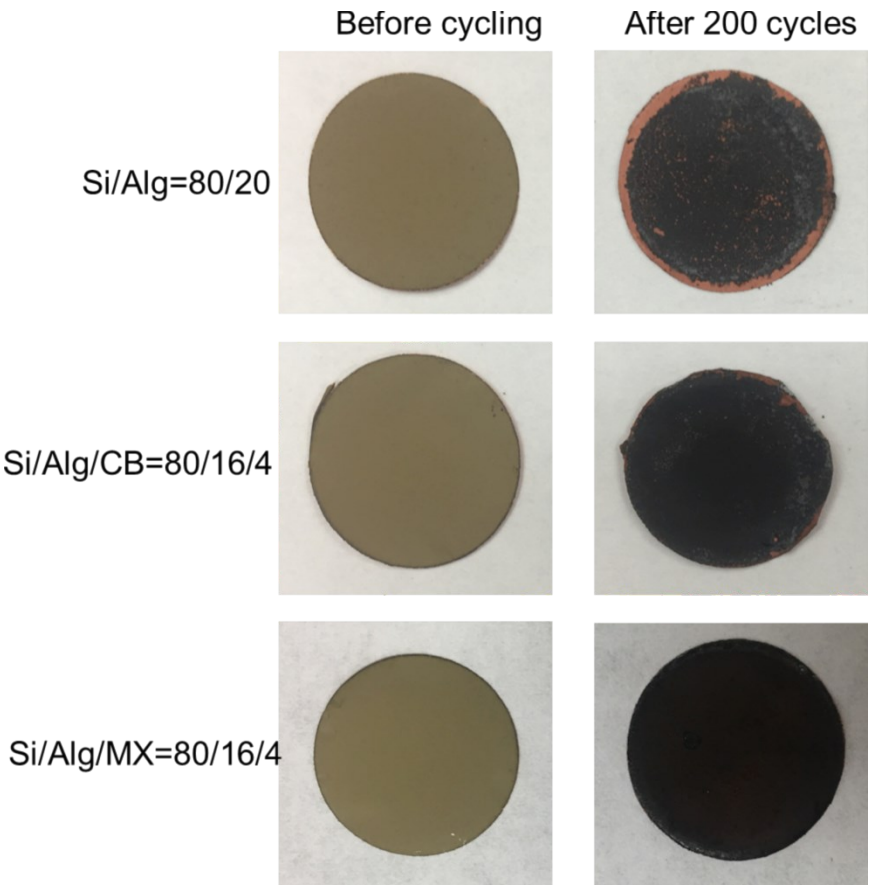

Figure S6. Digital images of Si/Alg, Si/Alg/CB, and Si/Alg/MX electrodes before and after cycling.

Table S1. Electronic conductivities of Alg/MX and Alg/CB polymer composites without any silicon nanoparticles. Four-point probe was used to determine resistance from which electronic conductivities were calculated.

Sample	80 % Alg + 20 % CB	90 % Alg + 10 % CB	80 % Alg + 20 % MX	90 % Alg + 10 % MX
Electronic conductivity (S/cm)	1.82×10^{-4}	Beyond detection limit	2.62×10^{-4}	1.00×10^{-6}

These samples were made without silicon nanoparticles.

Effect of Silicon Loading

We performed a study on the effect of silicon loading silicon anode performance. We made electrodes with low (0.38 mg/cm^2) and high (1.2 -2.2 mg/cm^2) silicon loading (Figure S7), along with electrodes with intermediate silicon loading (~0.7 mg/cm^2). The lowest loading electrodes demonstrated a capacity of 970 mAh/g_{Si} (776 mAh/g_{total}) at the 200th cycle at 0.5 C, which was higher than the electrode with intermediate loading. The high loading electrodes (1.2 mg/cm^2) exhibited the poorest capacities as compared to the other two silicon loadings tested. This is observed because of poor adhesion to the current collector, higher diffusion limitations, and larger stress generation in thicker (or higher loading) electrodes.[1] The adhesion effects with mass loading were confirmed by doing a peel testing. The adhesion of the highest loading electrode to the copper current collector was the poorest, followed by intermediate and low loading electrodes (Figure S8). We did not test the 1.8 mg/cm^2 and 2.2 mg/cm^2 loading electrodes because of very poor adhesion properties. Though the lowest loading electrodes delivered the highest capacities, it is unrealistic to use those for practical applications.[1]

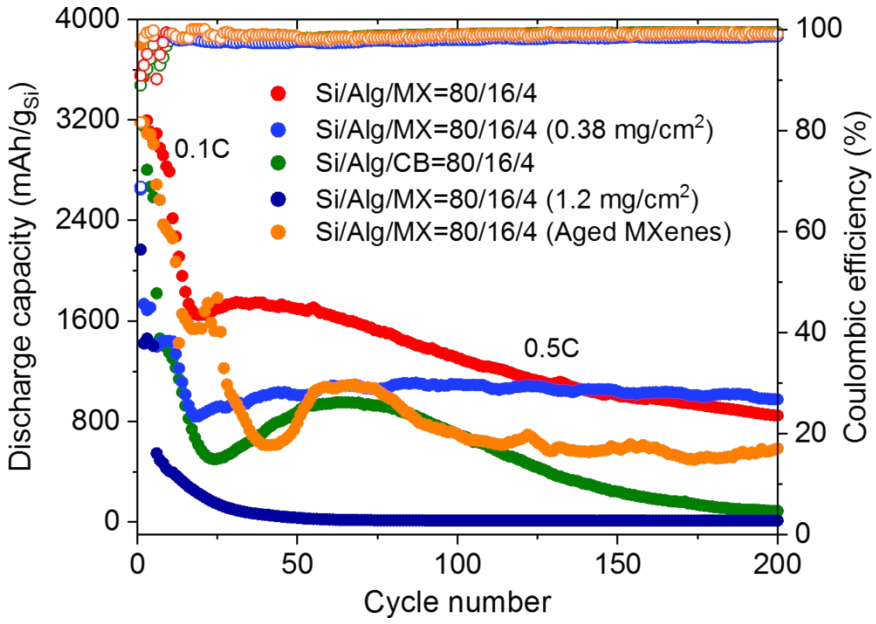

Figure S7. Cycling performance of silicon electrodes.

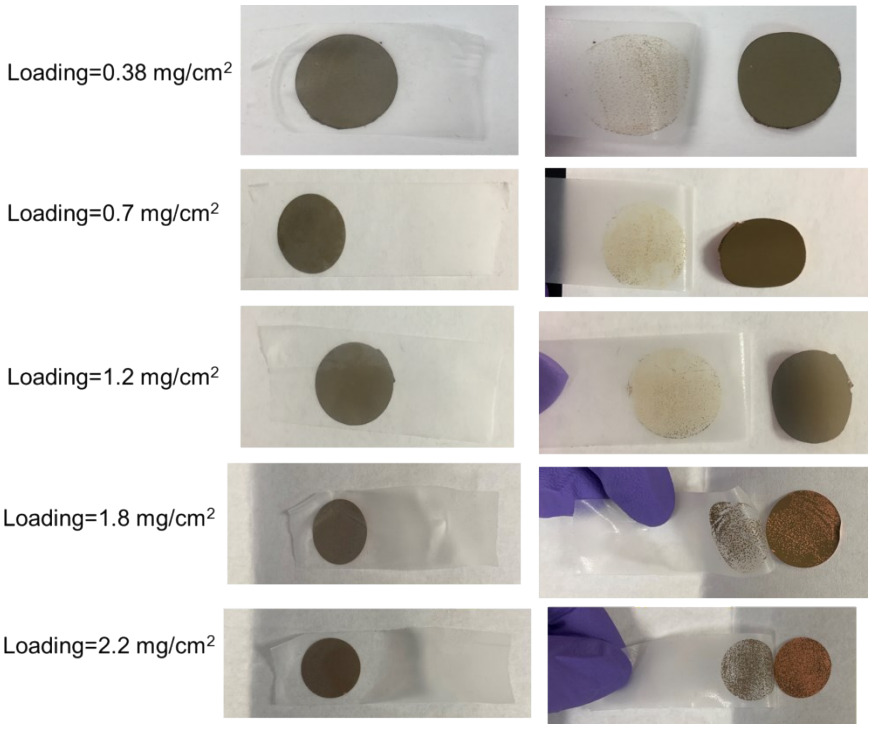

Figure S8. Tape test to determine peel strength test of Si/Alg/MX electrode with low (0.38 mg/cm^2), intermediate (0.7 mg/cm^2), and high (1.2-2.2 mg/cm^2) active material loadings.

Effect of MXene Aging

MXene nanosheets (in colloidal form in water) oxidize over time which causes drop in electronic conductivity due to degradation of MXene nanosheets to TiO_2.[2-3] To understand the effect of MXene oxidation on silicon anode performance, we compared silicon anodes that had been prepared with freeze-dried[2] MXenes that were aged for 20 days under vacuum at room temperature. All prior electrodes presented utilized fresh MXenes. As seen in Figure S7, the aged electrode had a capacity of ~590 mAh/g_{Si} at the 200th cycle, which was ~65% lower than the electrodes made with fresh MXenes. This result is expected because the storage method we employed does not completely ensure protection of MXenes from oxidation. Therefore, aging of the MXenes results in poorer silicon anode performance because of oxidation and a drop in conductivity.[4]

Electrochemical Impedance Spectroscopy

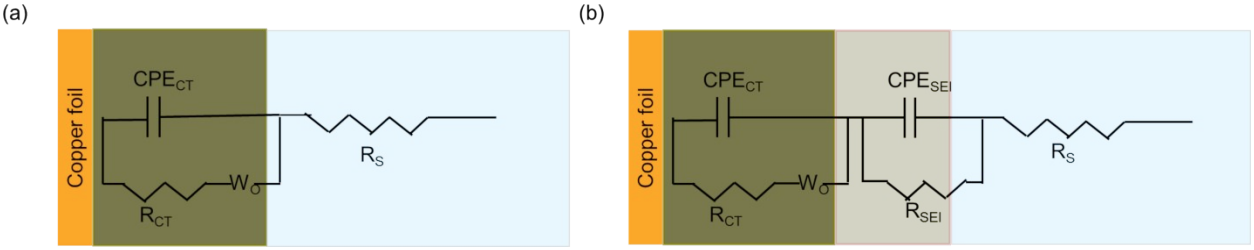

Figure S9. Equivalent circuits used for fitting the Nyquist data obtained from electrochemical impedance spectroscopy (EIS) (Figure 4 in main text) (a) before cycling (one time constant) and (b) after cycling (two time constants).

Table S2. Equivalent circuit fit values for the Nyquist plot (Figure 4 in main text and Figure S9) obtained from electrochemical impedance spectroscopy performed on Si/Alg, Si/Alg/CB, and Si/Alg/MX electrodes before cycling, after 10 and 50 cycles.

Before cycling							
	R_O (Ω)	R_{CT} (Ω)	CPE_{CT} (x10^{-5} F)	R_{SEI} (Ω)	CPE_{SEI} (x10^{-5} F)	σ (Ω/s)	D_{Li}^+ (x10^{-12} cm^2/s)
Si/Alg	3.3	116	3.5	-	-	-	-
Si/Alg/CB	0.8	104	400	-	-	-	-
Si/Alg/MX	1.2	51.4	6.3	-	-	-	-
After 10 cycles							
Si/Alg	1.2	5.1	121	7.8	4.3	9.1	3.26
Si/Alg/CB	0.7	17.9	8.7	107	339	50.7	0.15
Si/Alg/MX	1.0	2.5	1.4	5.6	18.4	9.4	20.2
After 50 cycles							
Si/Alg	1.2	18.9	830	10.2	6.4	6.7	0.78
Si/Alg/CB	1.0	1.4	3.6	139	329	47.3	0.08
Si/Alg/MX	1.0	3.0	0.9	5.4	22.5	8.4	26.9

Equivalent circuits were fit to the Nyquist plot (Figure 4) in the main text using the ZView software. The error value for each fit was less than 0.01 which implied that the model represented a good fit. The fitted values (R_O, R_{CT}, CPE, R_{SEI}) are represented in the table above (Table S1). Diffusion coefficient of Li^+ ions (D_{Li^+}) after 10 and 50 cycles was calculated using Eqn 1 and 2.

$$Z_{Re} = R_O + R_{CT} + \sigma\omega^{-0.5} \qquad ...(1)$$

$$D_{Li^+} = \frac{1}{1}\left[\left(\frac{V_M}{FS\sigma}\right)\left(\frac{dV}{dX}\right)\right]^2 \qquad ...(2)$$

Here, D_{Li+} is the diffusion coefficient (cm^2/s), ω is the radial frequency (s^{-1}), Z_{Re} is the real impedance, R_O is ohmic resistance, and R_{CT} is charge transfer resistance, V_M is the molar volume of silicon, F is Faraday's constant (96485 C/mol), S is the surface area of electrode (for simplicity, the geometric area of the electrode in cm^2 (2.01 cm^2) is used), σ is a parameter calculated from the slope of the plot of real impedance (Z_{Re}) *vs.* $\omega^{-0.5}$ (Figure S10a and Eqn 1), and dV/dx is the slope electrode potential (V) *vs.* Li ions in Si (X) plot (Figure S10b). The calculations were done following the previous reports.[5]

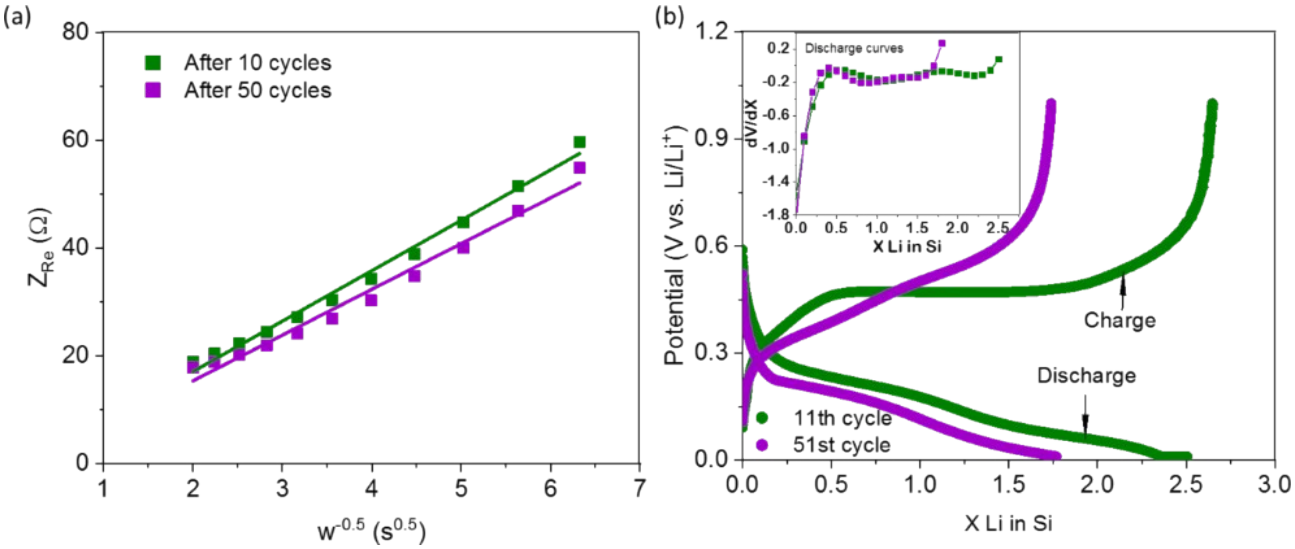

Figure S10. (a) Plot of real impedance (Z_{Re}) *vs.* $\omega^{-0.5}$. This graph is plotted from the Nyquist data in Figure 4. The slope of this plot gives the value of σ used for calculating solid state diffusion co-efficient of Li^+ ions using Eqn 2. (b) Plot of Potential (V) *vs.* X Li in silicon for 11th and 51st cycle at 0.5 C. Here, X is amount of Li ions in silicon. Inset shows a plot of dV/dX *vs.* X Li in silicon.

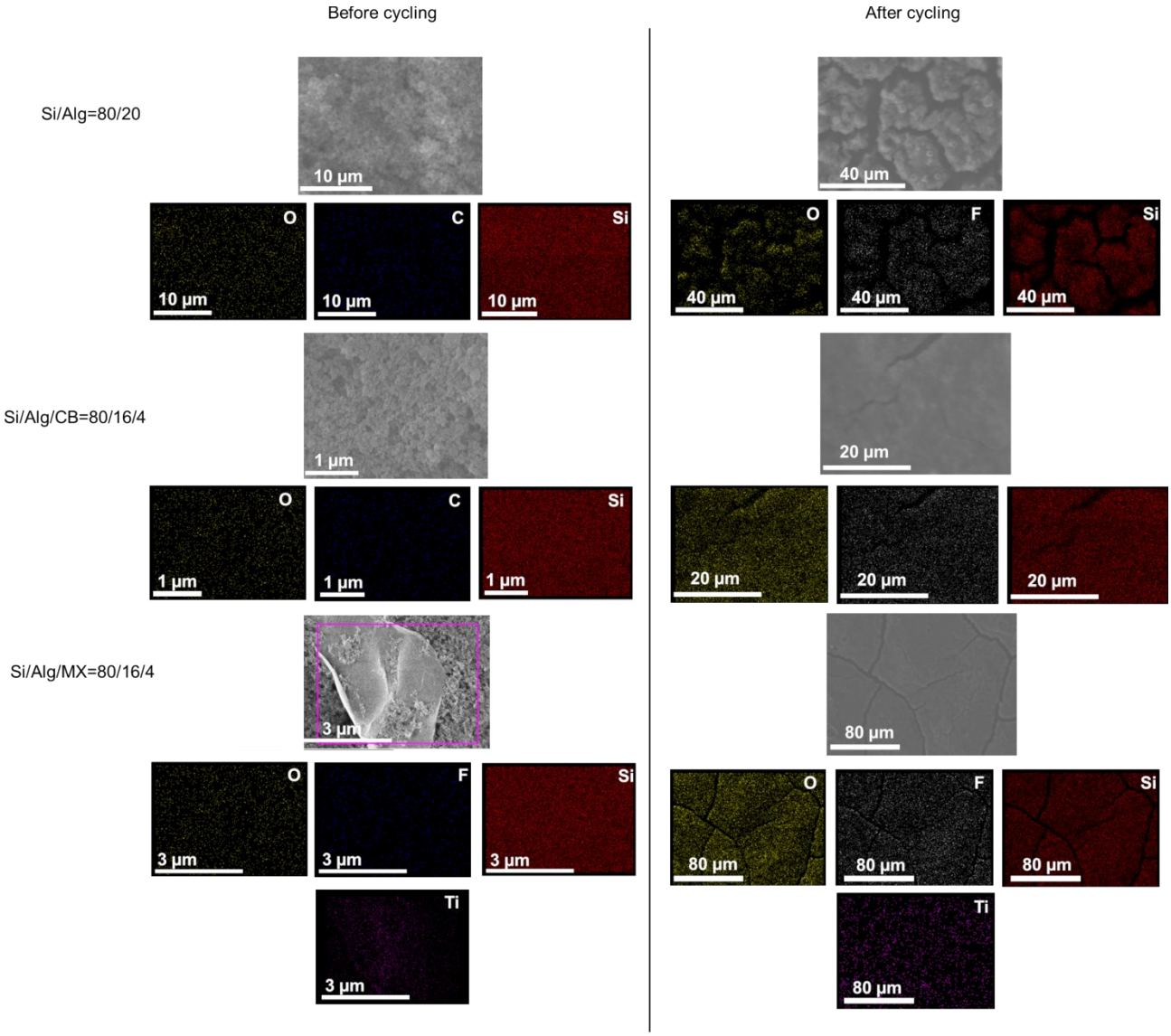

Figure S11: Energy dispersive X-ray spectroscopy (EDS) of Si/Alg, Si/Alg/CB, and Si/Alg/MX electrodes before and after cycling. For electrodes after cycling, the cells were disassembled in a glovebox and the electrodes were cleaned with dichloromethane to get rid of excess salts. These electrodes were then dried in vacuum at room temperature for 3 days. EDS was performed on JEOL JSM SEM equipment with an accelerating voltage of 20 kV and working distance of 8 mm.

XPS

X-ray photoelectron spectroscopy (XPS) was performed on Si/Alg, Si/Alg/CB, and Si/Alg/MX electrodes before and after 50 cycles. The XPS spectra were obtained using an Omicron ESCA Probe with a monochromated Mg Ka radiation. The survey scans (Figure S12) were conducted using a pass energy of 100–1,100 eV with steps of 1.0 eV and 50-ms dwell time. High-resolution scans (Figures S13-S15) were conducted at a pass energy of 150 eV with steps of 0.05 eV. A Shirley-type background correction was applied, and curve fitting was performed using a Gaussian-Lorentzian peak shape. As expected, all electrodes showed F 1s peak after cycling. The Ti 2p peak in Si/Alg/MX electrodes was not detectable due to very low concentration in entire electrode) of MXenes (4 wt%) in entire electrode. The electrodes after cycling demonstrated peaks from expected products of SEI, to name a few, LiF, Li_xPF_y, $CH_2OCOOLi$, *etc*.

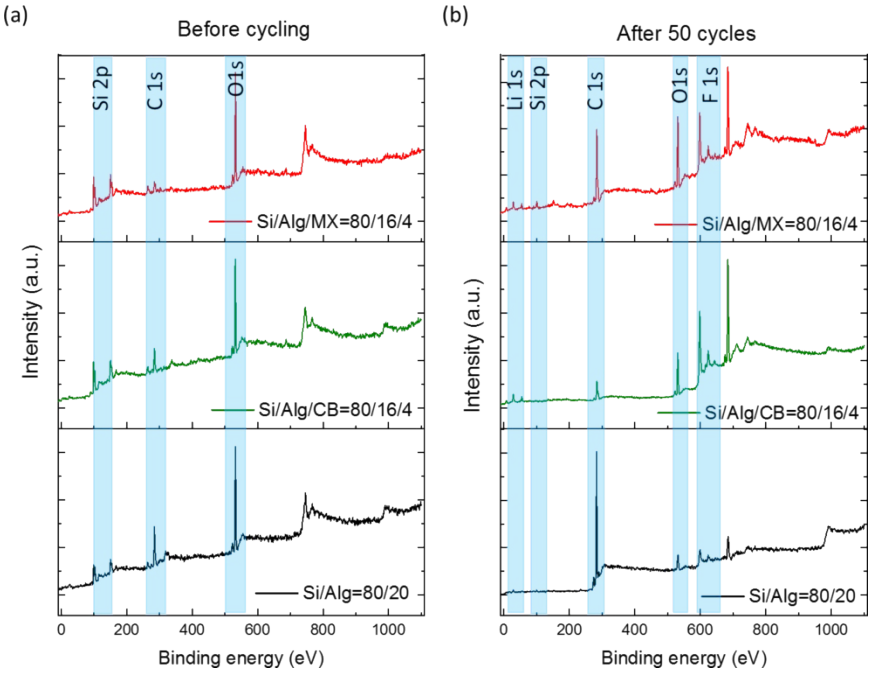

Figure S12: X-ray photoelectron spectroscopy survey scans for Si/Alg, Si/Alg/CB, and Si/Alg/MX electrodes (a) before and (b) after 50 cycles.

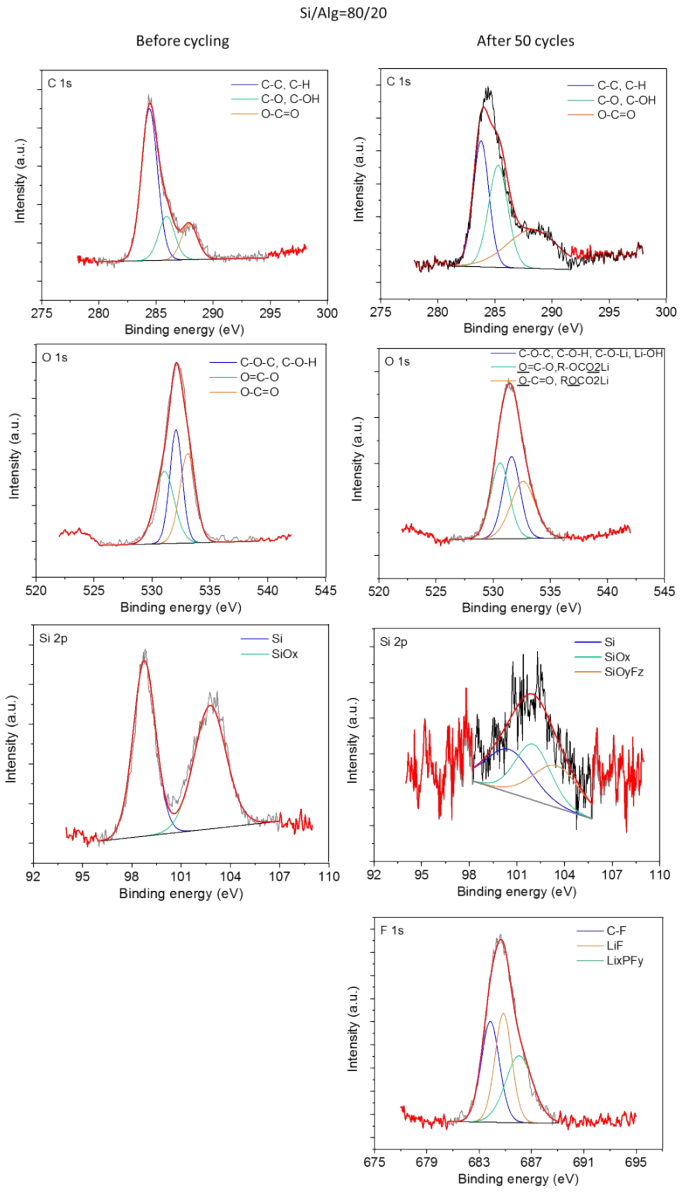

Figure S13. Deconvoluted C 1s, O 1s, Si 2p, and F 1s peaks for Si/Alg electrode before and after 50 cycles.

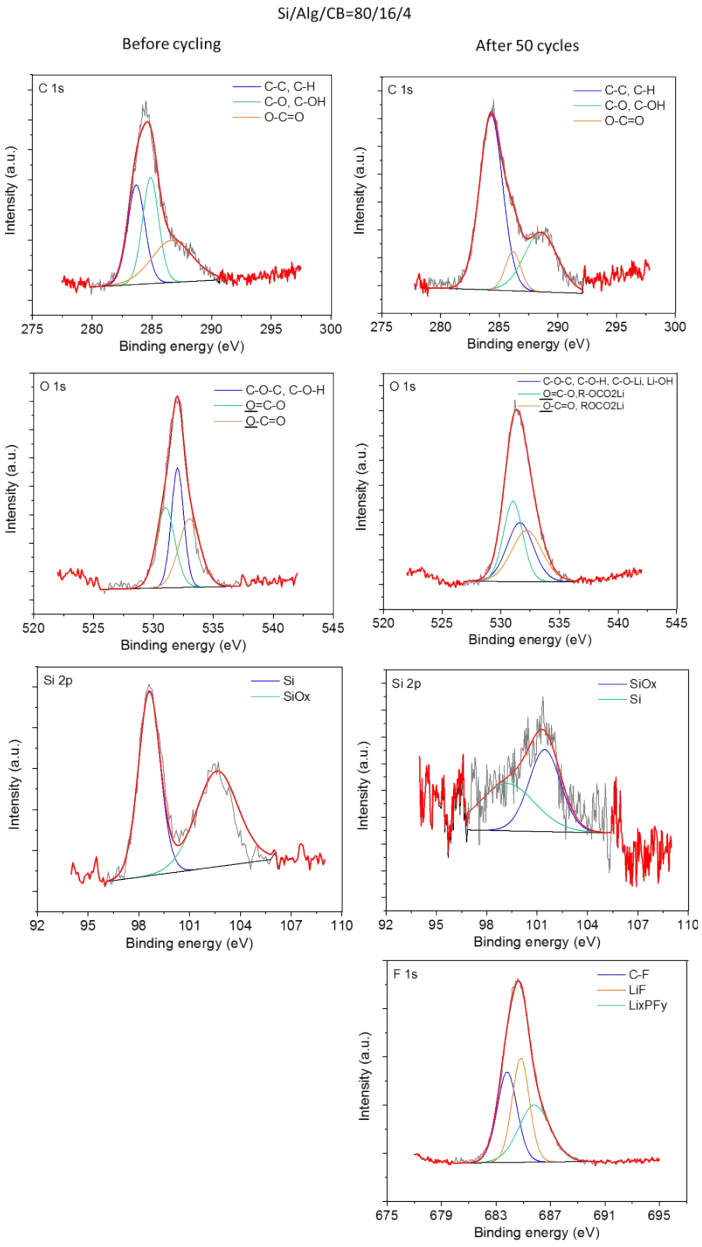

Figure S14. Deconvoluted C 1s, O 1s, Si 2p, and F 1s peaks for Si/Alg/CB electrode before and after 50 cycles.

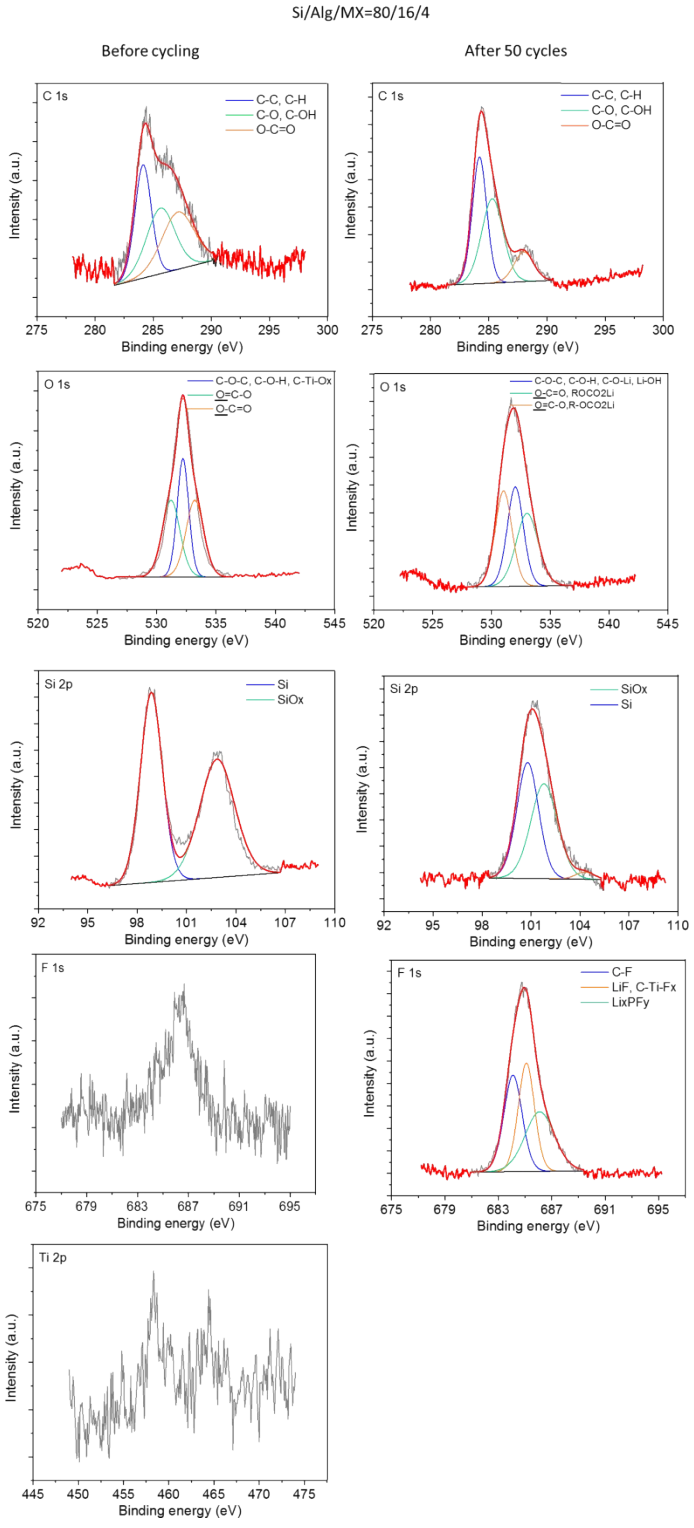

Figure S15. Deconvoluted C 1s, O 1s, Si 2p, and F 1s peaks for Si/Alg/MX electrode before and after 50 cycles.

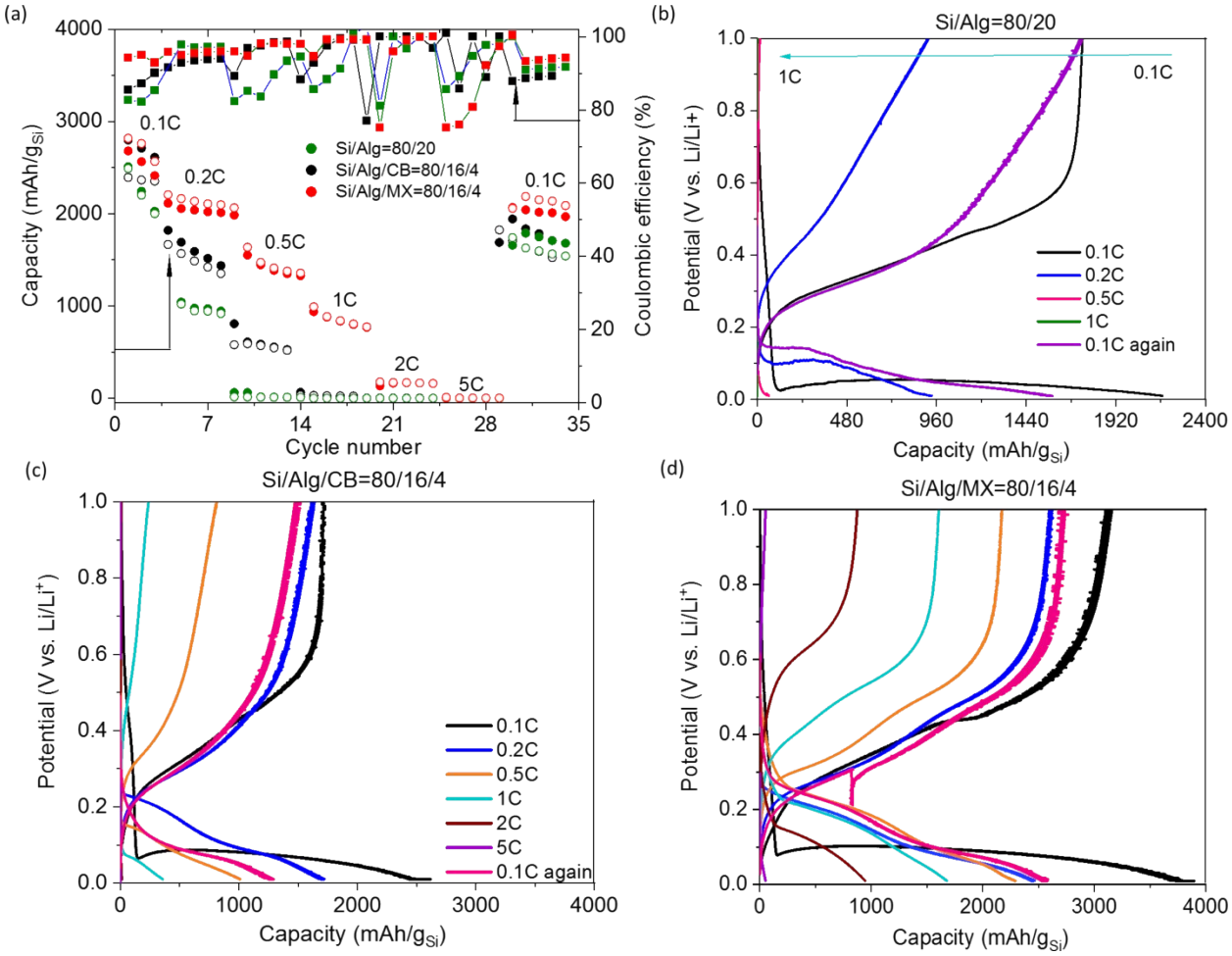

Figure S16. (a) Rate performance of Si/Alg, Si/Alg/CB, and Si/Alg/MX all combined in one graph. The C-rate was increased form 0.1 C to 5 C and then brought back to 0.1 C to determine the capacity recovery. Voltage profiles for the 1st cycle at every C-rate for (b) Si/Alg, (c) Si/Alg/CB, and (d) Si/Alg/MX electrode. The voltage profiles at 2 C and 5 C for Si/Alg are not shown because very few data points were collected at those C-rates.

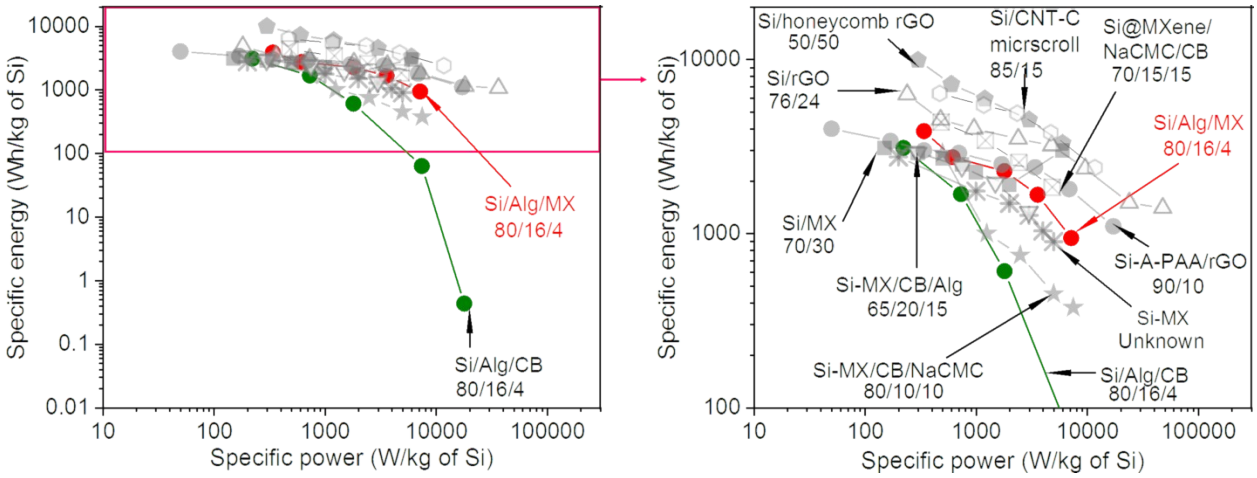

Figure S17. Ragone plot of silicon-based electrodes. Here, both specific energy and power are based on mass of silicon in electrode. The data shown in grey (filled and hollow) is taken form literature.[6-13]

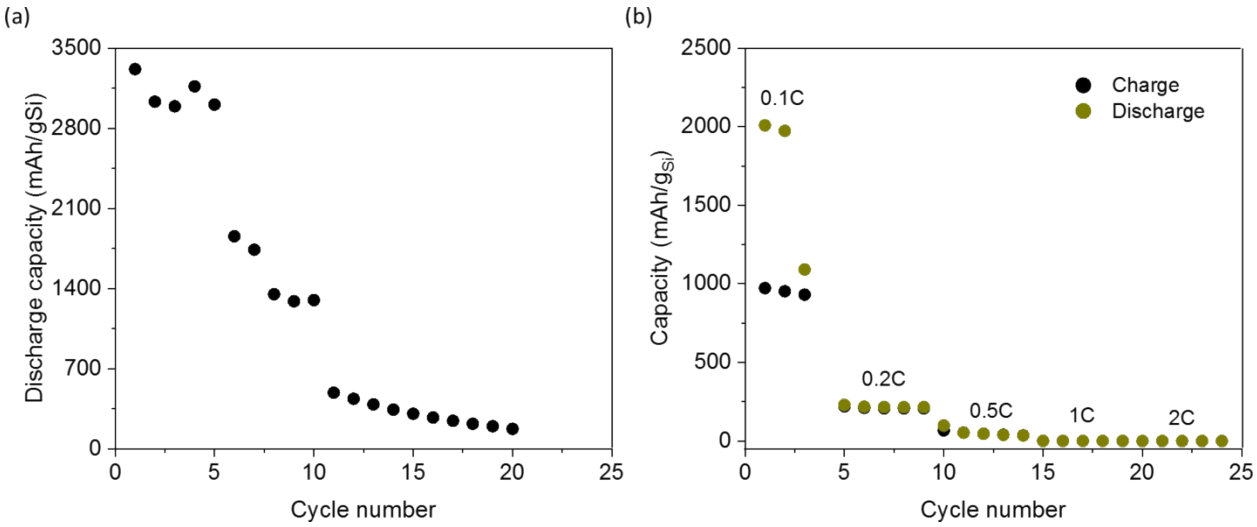

Figure S18. (a) Cycling performance of Si/MX=96/4 wt% electrodes without any sodium alginate binder. The cycling was performed at 0.1 C in CC-CV mode followed by 0.5 C in CC mode. (b) Rate performance of Si/MX=96/4 wt% at different C-rates.

A silicon-based electrode with 96 wt% Si and 4 wt% Mxenes was fabricated (same way as listed in electrode synthesis section). No binder was added here. The as-synthesized electrodes were then used to fabricate cells (same way as listed in electrochemical characterization section). The electrode demonstrated very poor cycling performance with capacity dropping to less than 150 mAh/g within 10 cycles. The rate performance was also poor, and the cell died after C-rate of 2 C (i.e. higher current values). This implies that 4 wt% MXenes alone are not enough to ensure electrode integrity and a binder is necessary.

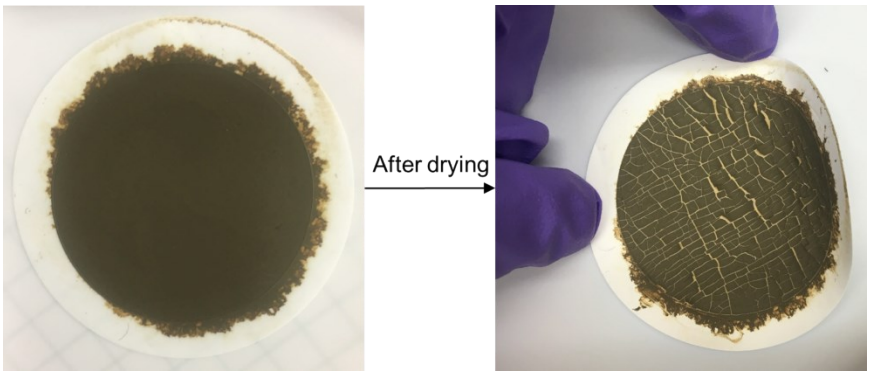

Figure S19. Images of Si/Alg/MX=80/16/4 dispersion vacuum filtered through Nylon membrane (left shows the image before drying and right shows the image after drying). The contents in the desired ratio were mixed in water to give a final concentration of 1 mg/ml. 40 ml of this solution was then vacuum filtered through the membrane.

Table S3. Table with values of specific energy and capacity (both normalized by mass of silicon and total electrode mass), MX content (wt%), Si content (wt%), and electrode composition.

Reference	Specific power (W/kg of Si)	Specific energy (Wh/kg of Si)	Long term cycling capacity	MX/rGO/C content	Si content (wt%)	Si loading (mg/cm^2)	Electrode composition	Specific power (W/kg total)	Specific energy (Wh/kg total)
This work	340.0	3880	900 mAh/g_{Si}, 720 mAh/gt_{otal} at 200th cycle at 0.5 C	MX=4 wt%	80	0.7	Si/Alg/MX= 80/16/4	270.0	3100
	615.0	2750						490.0	2200
	1790	2290						1430	1830
	3570	1670						2850	1340
	7150	945.0						5720	760.0
Ref. 37	300.0	2910	1700 mAh/g_{Si}, 1140 mAh/g_{total} at 200th cycle at ~0.14 C	MX= 22 wt%	43	0.45-0.6	Si-MX/CB/Alg =65/20/15	130.0	1270
	750.0	2420						325.0	1050
	1490	1960						650.0	850.0
	2990	1330						1300	580.0
Ref. 13	150.0	3100	1450 mAh/g_{Si}, 1015 mAh/g_{total} at 300th cycle at ~0.35 C	MX= 30 wt%	70	0.9	Si/MX=70/30	105.0	2170
	300.0	2900						210.0	2030
	500.0	2700						350.0	1890
	750.0	2500						530.0	1750
	1000	2250						700.0	1580
	2000	1900						1400	1330
	3000	1500						2100	1050
Ref. 36	500.0	2900	188 mAh/g_{Si}, 24 mAh/g_{total} at 150th cycle at ~0.05 C	MX= 66 wt%	13	0.1	Si-MX/CB/Na CMC =80/10/10	70.00	380.0
	1250	1000						162.5	130.0
	2500	750.0						330.0	100.0
	5000	450.0						650.0	60.00
	7500	400.0						980.0	50.00
Ref. 60	200.0	2750	2000 mAh/g_{Si} at 100th cycle at ~0.05 C	-	-	1-1.3	-	-	-
	1000	1750							
	2000	1490							
	3000	1270							
	4000	1030							
	5000	900.0							
Ref. 62	490.0	4400	400 mAh/gSi, 816 mAh/gtotal at 500th cycle at ~0.5 C	MX= 21 wt%	49	0.8-1	Si@MXene/ NaCMC/CB =70/15/15	240.0	2100
	1200	3400						600.0	1700
	2400	2600						1200	1300
	4900	1800						2400	900.0
Ref. 64	50	4000	1500 mAh/g_{Si}, 1050 mAh/g_{total} at 300th cycle at ~0.8 C	rGO= 10 wt%	76.5	1.1	Si-A-PAA/rGO =90/10	40.00	3060
	170	3400						130.0	2600
	340	3000						260.0	2300
	700	2900						355.0	2220
	1700	2500						1300	1900
	3400	2400						2600	1800
	6900	1800						5280	1400
	17200	1100						13160	840.0
Ref. 63	120.0	3150	765 mAh/g_{Si}, 580 mAh/g_{total} at 300th cycle at 3 C	rGO=24 wt%	76	0.12	Si/rGO=76/24	91.00	2400
	240.0	2250						182.0	1710
	480.0	2000						365.0	1520
	1200	1750						912.0	1330
	2400	1600						1820	1220
	4800	1180						3650	900.0

	12000	750						9120	570
Ref. 61	300	9900	2236 mAh/g_{Si}, 1118 mAh/g_{total} at 50th cycle at 0.01 C	rGO=50 wt%	50	1-1.6	Si/honeycomb rGO=50/50	150	4950
	600	7200						300	3600
	1200	5940						600	2970
	3000	4500						1500	2250
	6000	3300						3000	1650
Ref. 39	470.0	6380	2056 mAh/g_{Si}, 2420 mAh/g_{total} at 300th cycle at ~0.1 C	C=15 wt%	85	0.7-2	Si/CNT-C microscrolls =85/15	400	5420
	1180	5460						1000	4640
	2350	4910						2000	4170
	4710	3970						4000	3220
	11670	2390						10000	2030

The references are referred to the main text

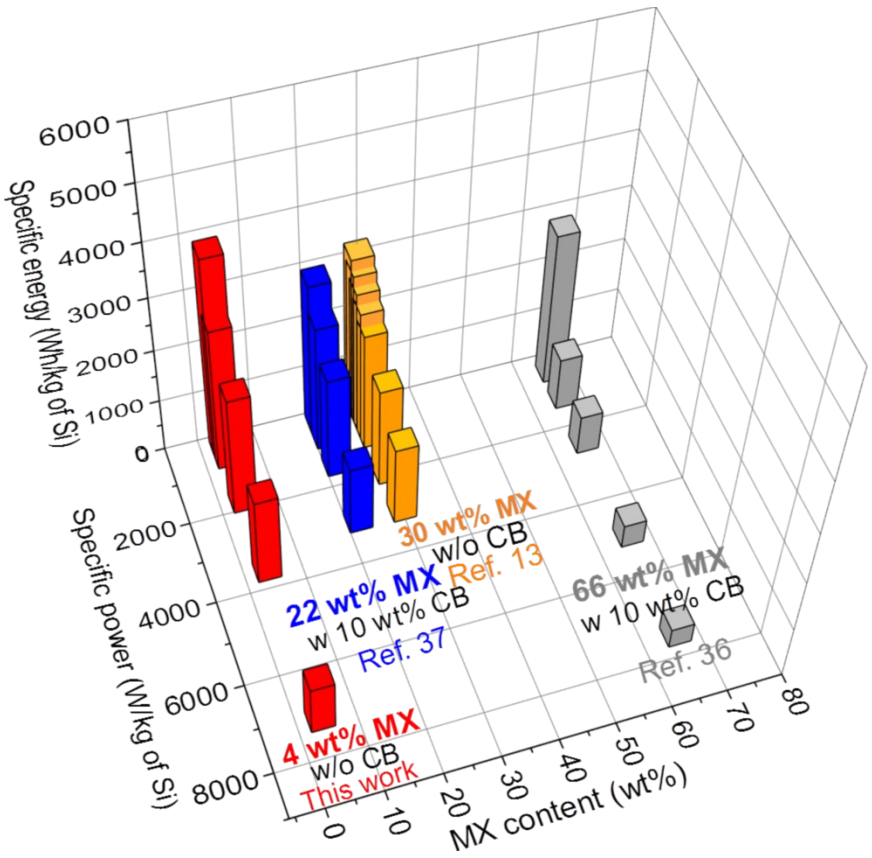

Figure S20. 3D plot with specific energy, specific power (both based on mass of silicon), and MXene content (wt%). The citations are referred to the main text.

References

1. Nitta, N.; Yushin, G., High-Capacity Anode Materials for Lithium-Ion Batteries: Choice of Elements and Structures for Active Particles. *Part. Part. Syst. Charact.* **2014,** *31* (3), 317-336.
2. Habib, T.; Zhao, X.; Shah, S. A.; Chen, Y.; Sun, W.; An, H.; Lutkenhaus, J. L.; Radovic, M.; Green, M. J., Oxidation Stability of $Ti_3C_2T_x$ MXene Nanosheets in Solvents and Composite Films. *npj 2D Mater. Appl.* **2019,** *3* (1).
3. Lotfi, R.; Naguib, M.; Yilmaz, D. E.; Nanda, J.; van Duin, A. C. T., A comparative Study on the Oxidation of Two-Dimensional Ti_3C_2 MXene Structures in Different Environments. *J. Mater. Chem. A* **2018,** *6* (26), 12733-12743.
4. Zhao, X.; Vashisth, A.; Prehn, E.; Sun, W.; Shah, S. A.; Habib, T.; Chen, Y.; Tan, Z.; Lutkenhaus, J. L.; Radovic, M.; Green, M. J., Antioxidants Unlock Shelf-Stable Ti_3C_2T (MXene) Nanosheet Dispersions. *Matter* **2019,** *1* (2), 513-526.
5. Xie, J.; Imanishi, N.; Zhang, T.; Hirano, A.; Takeda, Y.; Yamamoto, O., Li-ion Diffusion in Amorphous Si Films Prepared by RF Magnetron Sputtering: A Comparison of Using Liquid and Polymer Electrolytes. *Mater. Chem. Phys.* **2010,** *120* (2-3), 421-425.
6. Zhang, C.; Park, S.-H.; Seral-Ascaso, A.; Barwich, S.; McEvoy, N.; Boland, C. S.; Coleman, J. N.; Gogotsi, Y.; Nicolosi, V., High Capacity Silicon Anodes Enabled by MXene Viscous Aqueous Ink. *Nat. Commun.* **2019,** *10* (1).
7. Zhu, X.; Shen, J.; Chen, X.; Li, Y.; Peng, W.; Zhang, G.; Zhang, F.; Fan, X., Enhanced Cycling Performance of Si-MXene Nanohybrids as Anode for High Performance Lithium Ion Batteries. *Chem. Eng. J.* **2019,** *378*.
8. Kong, F.; He, X.; Liu, Q.; Qi, X.; Sun, D.; Zheng, Y.; Wang, R.; Bai, Y., Enhanced Reversible Li-ion Storage in $Si@Ti_3C_2$ MXene Nanocomposite. *Electrochem. Commun.* **2018,** *97*, 16-21.
9. Tian, Y.; An, Y.; Feng, J., Flexible and Freestanding Silicon/MXene Composite Papers for High-Performance Lithium-Ion Batteries. *ACS Appl. Mater. Interfaces* **2019,** *11* (10), 10004-10011.
10. Feng, K.; Ahn, W.; Lui, G.; Park, H. W.; Kashkooli, A. G.; Jiang, G.; Wang, X.; Xiao, X.; Chen, Z., Implementing an In-situ Carbon Network in Si/reduced Graphene Oxide for High Performance Lithium-ion Battery Anodes. *Nano Energy* **2016,** *19*, 187-197.
11. Chang, J.; Huang, X.; Zhou, G.; Cui, S.; Hallac, P. B.; Jiang, J.; Hurley, P. T.; Chen, J., Multilayered Si Nanoparticle/Reduced Graphene Oxide Hybrid as a High-Performance Lithium-Ion Battery Anode. *Adv. Mater.* **2014,** *26* (5), 758-64.
12. Tang, H.; Tu, J.-p.; Liu, X.-y.; Zhang, Y.-j.; Huang, S.; Li, W.-z.; Wang, X.-l.; Gu, C.-d., Self-assembly of Si/honeycomb Reduced Graphene Oxide Composite Film as a Binder-free and Flexible Anode for Li-ion Batteries. *J. Mater. Chem. A* **2014,** *2* (16), 5834-5840.
13. Wang, H.; Fu, J.; Wang, C.; Wang, J.; Yang, A.; Li, C.; Sun, Q.; Cui, Y.; Li, H., A Binder-free High Silicon Content Llexible Anode for Li-ion Batteries. *Energy Environ. Sci.* **2020,** *13* (3), 848-858.